

# Proximate Kitaev system for an intermediate magnetic phase in in-plane magnetic fields

Beom Hyun Kim,<sup>1</sup> Shigetoshi Sota,<sup>2</sup> Tomonori Shirakawa,<sup>2</sup> Seiji Yunoki,<sup>2,3,4</sup> and Young-Woo Son<sup>1</sup>

<sup>1</sup>*Korea Institute for Advanced Study, Seoul 02455, South Korea*

<sup>2</sup>*Computational Materials Science Research Team,*

*RIKEN Center for Computational Science (R-CCS), Kobe, Hyogo 650-0047, Japan*

<sup>3</sup>*Computational Condensed Matter Physics Laboratory,*

*RIKEN Cluster for Pioneering Research (CPR), Saitama 351-0198, Japan*

<sup>4</sup>*Computational Quantum Matter Research Team, RIKEN,*

*Center for Emergent Matter Science (CEMS), Wako, Saitama 351-0198, Japan*

(Dated: October 8, 2020)

Motivated by the magnetic phase transition of a proximate Kitaev system  $\alpha$ -RuCl<sub>3</sub> in the presence of a magnetic field, we study the simplest but essential quantum spin model with the ferromagnetic nearest neighboring (NN) Kitaev interaction and additional antiferromagnetic third NN Heisenberg interaction. Employing both exact diagonalization and density matrix renormalization group methods, we demonstrate that the model shows the magnetic phase transition from the zigzag order phase to the spin polarized phase through an intermediate phase in both cases when an in-plane magnetic field is applied perpendicular to the NN bond direction and when an out-of-plane field is applied, in good agreement with experimental observations. Furthermore, we verify that additional symmetric off-diagonal  $\Gamma$  interaction and ferromagnetic Heisenberg interaction between NN spins can both suppress the intermediate phase with the in-plane field. Our result gives important clues on determining relevant interactions in the field-induced magnetic phase transition of proximate Kitaev systems.

*Introduction* – Quantum spin liquid (QSL) is an exotic quantum phase in which any magnetic long-range order is prevented due to strong quantum fluctuation<sup>1</sup>. The Kitaev model with directional Ising-type interactions between the nearest neighboring (NN) spins (Kitaev interaction) in a honeycomb lattice is an exactly solvable system to host as the ground state the QSL phase interpreted with free Majorana fermions in a static  $Z_2$  gauge field<sup>2</sup>. For the last decade, there have been considerable efforts devoted to search materials hosting the Kitaev interaction<sup>3–5</sup>.

Among those candidates,  $4d/5d$ -based honeycomb systems such as  $\alpha$ -RuCl<sub>3</sub> and Na<sub>2</sub>IrO<sub>3</sub> were proposed as best ones to have strong Kitaev interactions<sup>6,7</sup>. While such systems certainly possess the predominant Kitaev interaction, their magnetic ground state has been turned out to be not the Kitaev spin liquid (KSL) but an antiferromagnetic (AFM) phase with the zigzag order<sup>8,9</sup>. Other non-negligible types of magnetic interactions such as Heisenberg interactions and symmetric off-diagonal  $\Gamma$  interactions [see Eq. (1)] have been known to play a role in determining the non-Kitaev ground state<sup>10,11</sup>.

Despite its long-range magnetic order,  $\alpha$ -RuCl<sub>3</sub> has been thought as a proximate Kitaev system<sup>12</sup>. Recent experiments with inelastic neutron scattering and Raman spectroscopy evidenced magnetic continuum excitations attributed to possible fractionalized Majorana fermions<sup>13–16</sup>. A fractionalized magnetic entropy has been also observed in specific heat measurements<sup>16,17</sup>. Moreover, a lot of experimental studies have supported that the zigzag order can be suppressed and an intermediate phase (IP), possible QSL, can emerge in between the zigzag spin order and the spin polarized order when an

external magnetic field is applied<sup>18–31</sup>. This IP has been recently reported to appear in the in-plane field (especially  $a$ -axis field) as well as the out-of-plane field<sup>28,30,31</sup>. An observed half-integer quantized plateau in thermal Hall conductivity has highly promoted that an anticipated IP would be the KSL<sup>26,31</sup>. The nature and origin of the IP are still under debate.

The effective model for  $\alpha$ -RuCl<sub>3</sub> in the presence of an external magnetic field has been proposed with the following Hamiltonian:

$$\begin{aligned}
 H = & \sum_{\gamma\langle i,j\rangle_\gamma} [J\mathbf{S}_i \cdot \mathbf{S}_j + K S_{i\gamma} S_{j\gamma} + \Gamma (S_{i\alpha} S_{j\beta} + S_{i\beta} S_{j\alpha})] \\
 & + \sum_{\gamma\langle i,j\rangle_\gamma} \Gamma' (S_{i\alpha} S_{j\gamma} + S_{i\gamma} S_{j\alpha} + S_{i\beta} S_{j\gamma} + S_{i\gamma} S_{j\beta}) \\
 & + \sum_{\langle\langle i,j\rangle\rangle} J_3 \mathbf{S}_i \cdot \mathbf{S}_j - \mu_B \sum_i \vec{h} \cdot \mathbf{g} \cdot \vec{S}_i, \quad (1)
 \end{aligned}$$

where  $\mathbf{S}_i$  is the spin-1/2 operator at site  $i$  with its  $\gamma$  ( $= x, y, z$ ) component  $S_{i\gamma}$ ,  $\langle i, j \rangle_\gamma$  stands for the NN pair of sites  $i$  and  $j$  along the  $\gamma$  bond, and  $\alpha$  and  $\beta$  refer to the two remaining coordinates other than  $\gamma$  [see Fig. S1(b) in Supplemental Material (SM)<sup>32</sup>].  $K$  and  $J$  are Kitaev and Heisenberg interactions, respectively,  $\Gamma$  and  $\Gamma'$  are two types of symmetric off-diagonal interactions, and  $J_3$  is Heisenberg interaction between the 3rd NN sites.  $\vec{h}$  is the external magnetic field,  $\mathbf{g}$  is the  $g$  tensor, and  $\mu_B$  is the Bohr magneton. For simplicity, we assume an isotropic  $g$  tensor, although both fairly isotropic and highly anisotropic ones have been proposed before<sup>33,34</sup>.

Until now, various models, in which specific parameters are set to zero in the general model given in Eq. (1),

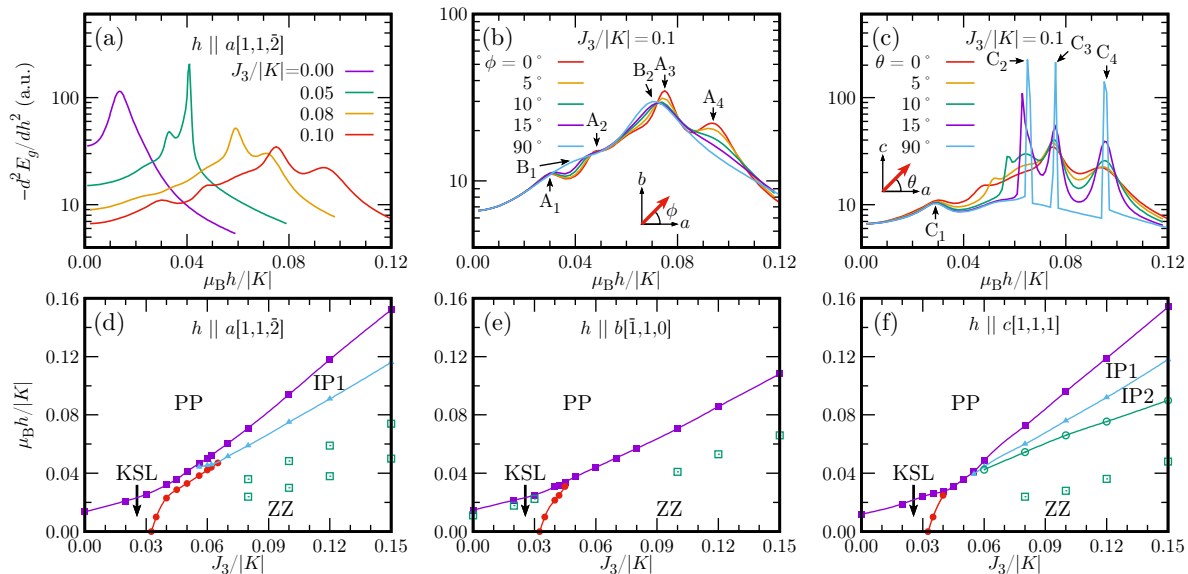


FIG. 1. (a) Second derivative of the ground state energy ( $d^2E_g/dh^2$ ) with respect to the magnetic field  $h$  along the  $a$  axis ( $[1,1,\bar{2}]$  direction<sup>32</sup>) for various values of the third nearest neighboring interaction  $J_3$ . (b)–(c) Second derivative of the ground state energy for various field directions (b) in the  $ab$  plane and (c) in the  $ac$  plane when  $J_3 = 0.1|K|$ . Here,  $\phi$  and  $\theta$  refer to angles between the  $a$  axis and the field direction in the  $ab$  and  $ac$  planes, respectively. (d)–(f) Ground state magnetic phase diagrams as a function of the external magnetic field  $h$  along (d) the  $a$  axis, (e) the  $b$  axis ( $[\bar{1},1,0]$  direction<sup>32</sup>), and (f) the  $c$  axis ( $[1,1,1]$  direction<sup>32</sup>). ‘ $A_{1-4}$ ’, ‘ $B_{1-2}$ ’, and ‘ $C_{1-4}$ ’ in (b) and (c) represent peaks of  $-d^2E_g/dh^2$  in the  $a$ -,  $b$ -, and  $c$ -axis fields, respectively. ‘KSL’, ‘ZZ’, ‘PP’, and ‘IP1 (IP2)’ in (d)–(f) refer to the Kitaev spin liquid, zigzag order, polarized phase, and intermediate phase, respectively. Green squares indicate peak positions corresponding to peaks  $A_1$  and  $A_2$  in (d),  $B_1$  in (e), and  $C_1$  in (f). All results are obtained for the  $K$ - $J_3$  model with  $K < 0$  calculated on a periodic 24-site cluster using the ED method<sup>32</sup>.

such as  $J$ - $K$ <sup>15,35</sup>,  $K$ - $\Gamma$ <sup>36–39</sup>,  $K$ - $\Gamma$ - $\Gamma'$ <sup>40,41</sup>, and  $J$ - $K$ - $\Gamma$ - $J_3$  models<sup>42,43</sup>, have been adopted to explore the magnetic properties of  $\alpha$ - $\text{RuCl}_3$ . Extended models including additional interactions have also been introduced in some literatures<sup>34,44–48</sup>. Among them, some are based on the AFM Kitaev interaction ( $K > 0$ ). In this case, an intermediate  $U(1)$  QSL phase is stabilized regardless of the direction of the field<sup>49</sup>. The  $K$ - $J$  model exhibits the zigzag order when  $K > 0$  and  $J < 0$ , and a clear IP, putative  $U(1)$  QSL, can appear in the external field along the  $c$  axis ( $[1,1,1]$  direction in terms of local coordinates of spins depicted in Fig. S1(a) in SM<sup>32</sup>)<sup>35</sup>. However, recent consensus is that the ferromagnetic (FM) Kitaev interaction ( $K < 0$ ) is more likely in  $\alpha$ - $\text{RuCl}_3$ <sup>11,16,25,34,42,50</sup>. The models with  $K < 0$  have also been employed to explain the zigzag order and the IP in the external field. The  $K$ - $\Gamma$ - $\Gamma'$  model with  $K < 0$ ,  $\Gamma > 0$ , and  $\Gamma' < 0$  studied recently successfully gives the IP in the field along the  $c$  axis. However, the IP is totally missing when the field is along the  $a$  axis ( $[1,1,\bar{2}]$  direction<sup>32</sup>)<sup>40,41</sup>. Numerical calculations for the  $J$ - $K$ - $\Gamma$ - $J_3$  model with  $K < 0$  also failed to show the IP in the  $a$ -axis field<sup>43</sup>.

In this study, we propose a simple theoretical quantum model only with  $K (< 0)$  and  $J_3 (> 0)$  to exhibit a genuine IP in both in-plane and out-of-plane magnetic fields. With the help of exact diagonalization (ED) and density matrix renormalization group (DMRG) methods, we demonstrate that the IP evidently manifests itself in

the field along both  $a$  and  $c$  axes, whereas it collapses in the field along the  $b$  axis ( $[\bar{1},1,0]$  direction<sup>32</sup>), in accordance with recent experiments<sup>27,30</sup>. Compared with other models to explain the ground state with the zigzag order, we assert the important role of the 3rd NN interaction in the most promising Kitaev material  $\alpha$ - $\text{RuCl}_3$ .

*Phase diagram of  $K$ - $J_3$  model* – According to the ED calculation with a  $C_3$  rotationally symmetric 24-site cluster [see SM<sup>32</sup>], the  $K$ - $J_3$  model exhibits the phase transition from the KSL to the zigzag order phase at  $J_3/|K| \approx 0.033$ . When the external magnetic field is applied, the KSL or zigzag order phase is suppressed and the spin polarized phase is eventually stabilized in the strong field limit. Figure 1(a) shows the second derivative of the ground state energy,  $d^2E_g(h)/dh^2$ , with respect to the  $a$ -axis field for the KSL ( $J_3/|K| = 0$ ) and the zigzag order ( $J_3/|K| = 0.05, 0.08$ , and  $0.1$ ) phases. Note that  $-d^2E_g(h)/dh^2$  is proportional to the magnetic susceptibility. Our calculation clearly shows the emergence of the IP during the phase transition from the zigzag order to the polarized phase whereas the KSL phase transforms directly to the polarized phase without any IP.

We further investigate the magnetic phase transition with various field directions. Figures 1(b) and 1(c) show  $-d^2E_g(h)/dh^2$  for  $J_3/|K| = 0.1$  when the field direction varies from the  $a$  to  $b$  axis in the  $ab$  plane and from the  $a$  to  $c$  axis in the  $ac$  plane, respectively. Interestingly, peak  $A_4$  associated with the highest critical field

at  $\mu_B h = 0.094|K|$  gradually diminishes when the field direction is away from the  $a$  to  $b$  axis. This peak becomes indistinguishable when  $\phi = 15^\circ$ , where  $\phi$  is an angle between the field direction and the  $a$  axis in the  $ab$  plane. Only peak B<sub>2</sub> at  $\mu_B h = 0.071|K|$  remains with a small satellite (peak B<sub>1</sub>) at  $\mu_B h = 0.041|K|$  in the  $b$ -axis field. In terms of the symmetry of the  $K$ - $J_3$  model, the IP appears (disappears) when the field is applied perpendicular (parallel) to one of three possible NN bonds, in good accordance with recent experiments of  $\alpha$ -RuCl<sub>3</sub><sup>28,31</sup>.

In contrast, when the field direction varies from the  $a$  to  $c$  axis in Fig. 1(c), the two highest peaks (peaks A<sub>3</sub> and A<sub>4</sub>) are robust with even reducing their peak widths until the field points close to the  $[1, 1, \bar{1}]$  direction, which corresponds to an angle  $\theta$  between the field direction and the  $a$  axis in the  $ac$  plane being about  $19.47^\circ$  ( $\approx \cos^{-1} \frac{2\sqrt{2}}{3}$ ). Concomitantly, a new peak (peak C<sub>2</sub>) appears around  $\mu_B h = 0.066|K|$ . This directly indicates the emergence of additional IP when the field is applied out of the  $ab$  plane. Because the  $K$ - $J_3$  model is invariant under the  $z$ -component reversal of all spins ( $S_{iz} \rightarrow -S_{iz}$ ),  $-d^2 E_g(h)/dh^2$  is exactly the same in both magnetic fields along the  $[1, 1, \bar{1}]$  direction and the  $[1, 1, 1]$  direction ( $c$  axis). Therefore, the IPs determined by peaks A<sub>3</sub> and A<sub>4</sub> in the  $a$ -axis field, and peaks C<sub>3</sub> and C<sub>4</sub> in the  $c$ -axis field are adiabatically equivalent.

We should remark that peaks labeled as A<sub>1</sub> (at  $\mu_B h \approx 0.03|K|$ ), A<sub>2</sub> ( $0.048|K|$ ), B<sub>1</sub> ( $0.041|K|$ ), and C<sub>1</sub> ( $0.028|K|$ ) in Figs. 1(b) and 1(c), appearing in a small field region where the zigzag order still remains, are not related to the phase transition but due to the finite size effect [see SM<sup>32</sup>]. We also confirm that the emergence of IP in both  $a$ - and  $c$ -axis fields is robust in the ED calculation with a different cluster geometry, although the number of IPs in the  $c$ -axis field may depend on the cluster geometry [see SM<sup>32</sup>].

Figures 1(d)–1(f) show the ground state phase diagrams of the  $K$ - $J_3$  model for three different field directions. In these phase diagrams, the following features are noticeable: i) The intermediate KSL phase is extended from  $J_3/|K| \approx 0.033$  to  $0.065$  in the presence of the  $a$ -axis field but it progressively shrinks in other field directions. ii) The IPs, emerging in both  $a$ - and  $c$ -axis fields, are distinct from the KSL phase, while any IP is inhibited in the  $b$ -axis field. iii) In the  $c$ -axis field, two consecutive IPs occur and the one (IP1) appearing in the larger field is adiabatically equivalent to the IP found in the presence of the  $a$ -axis field.

*DMRG calculation* – For the robustness of our ED results shown above, especially to check the finite size effect, we perform the DMRG calculation with a periodic 32-site cluster. The DMRG method is believed to accurately simulate the ground state of the  $K$ - $J_3$  model even in the two dimensional limit [see SM<sup>32</sup>].

Figure 2(a) shows  $-d^2 E_g/dh^2$  for  $J_3/|K| = 0.1$  in the  $a$ -,  $b$ -, and  $c$ -axis fields. Noteworthy, there is no peak of  $-d^2 E_g/dh^2$  below  $\mu_B h/|K| = 0.05$  in any field direction. With this, we can assure that the low-field peaks

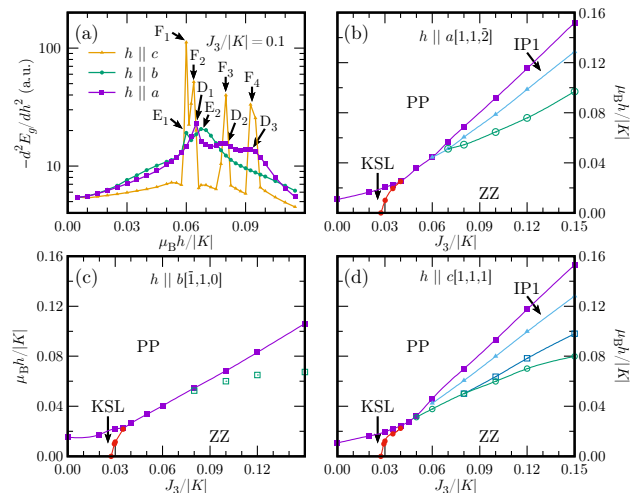


FIG. 2. (a) Second derivative of the ground state energy ( $d^2 E_g/dh^2$ ) with respect to the  $a$ -,  $b$ -, and  $c$ -axis fields  $h$  when  $J_3/|K| = 0.1$ . (b)–(d) Ground state magnetic phase diagrams as a function of the external magnetic field  $h$  along (b) the  $a$  axis, (c) the  $b$  axis, and (c) the  $c$  axis. ‘D<sub>1–3</sub>’, ‘E<sub>1,2</sub>’, and ‘F<sub>1–4</sub>’ in (a) represent peaks of  $-d^2 E_g/dh^2$  in the  $a$ -,  $b$ -, and  $c$ -axis fields, respectively. Green squares indicate peak positions corresponding to peak E<sub>1</sub> in (c). All results are obtained for the  $K$ - $J_3$  model with  $K < 0$  calculated on a periodic 32-site cluster using the DMRG method<sup>32</sup>.

below  $\mu_B h/|K| = 0.05$  in the ED calculation are due to the finite size effect and do not involve any phase transition. Above  $\mu_B h/|K| = 0.05$ , the DMRG calculation finds three (D<sub>1</sub>, D<sub>2</sub>, and D<sub>3</sub>), two (E<sub>1</sub> and E<sub>2</sub>), and four peaks (F<sub>1</sub>, F<sub>2</sub>, F<sub>3</sub>, and F<sub>4</sub>) of  $-d^2 E_g/dh^2$  in the  $a$ -,  $b$ -, and  $c$ -axis fields, respectively, in contrast with the ED calculation in which two, one, and three peaks appear, respectively. Two and three types of consecutive IPs seem to be manifested in the  $a$ - and  $c$ -axis fields, respectively. In the  $b$ -axis field, there exist two peaks (peaks E<sub>1</sub> and E<sub>2</sub>). The lower peak (peak E<sub>1</sub>), however, is not related to the phase transition since it extends into the zigzag phase in larger  $J_3/|K|$  cases. As in the ED calculation, the higher peak (peak E<sub>2</sub>) determines the phase boundary between the zigzag order and polarized phases. Positions of highest two peaks (peaks D<sub>2</sub> and D<sub>3</sub>) in the  $a$ -axis field and those of highest two peaks (peaks F<sub>3</sub> and F<sub>4</sub>) in the  $c$ -axis field are almost coincident with each other. Therefore, our DMRG calculation further supports the adiabatic equivalence between the two IPs (indicated as IP1 in Fig. 2) appearing in the presence of the fields along the two directions.

The phase diagrams obtained by the DMRG calculation is summarized in Figs. 2(b)–2(d) for three different field directions. Overall shapes are similar to those obtained by the ED calculation. As shown in Fig. 2(b), however, the intermediate KSL phase does not exist for  $0.04 \lesssim \mu_B h \lesssim 0.06$  in the  $a$ -axis field, different from the result of the ED calculation shown in Fig. 1(d). We suspect that such a difference would result from the finite

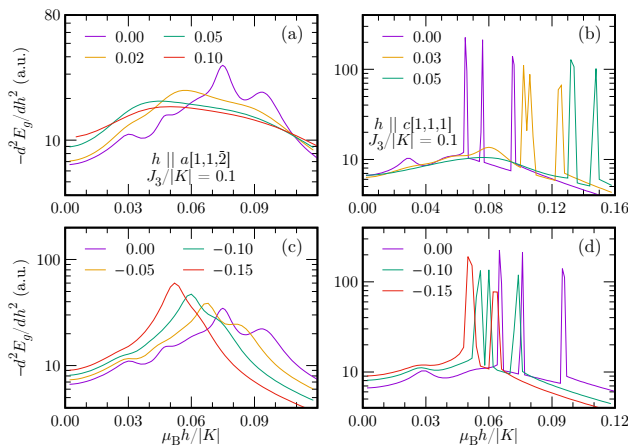


FIG. 3. Second derivative of the ground state energy ( $d^2 E_g / dh^2$ ) with respect to the magnetic field  $h$  along (a) the  $a$  axis for  $\Gamma/|K| = 0, 0.02, 0.05$ , and  $0.1$ , (b) the  $c$  axis for  $\Gamma/|K| = 0, 0.03$ , and  $0.05$ , (c) the  $a$  axis for  $J/|K| = 0, -0.05, -0.1$ , and  $-0.15$ , and (d) the  $c$  axis for  $J/|K| = 0, -0.1$ , and  $-0.15$ , when  $J_3/|K| = 0.1$ . All results are obtained for the  $K$ - $J_3$  model with  $K < 0$  calculated on a periodic 24-site cluster using the ED method<sup>32</sup>.

size effect. Moreover, it is not clear how many consecutive IPs exist in the  $a$ - and  $c$ -axis fields because the 32-site calculation also suffers from the finite size effect. Nevertheless, our study unambiguously reveals that the IP is evident both in the  $a$ - and  $c$ -axis fields but it is absent in the  $b$ -axis field.

*Discussion* – As described in Eq. (1), the relevant form of the magnetic interaction in  $\alpha$ - $\text{RuCl}_3$  has been believed to be more complex than the  $K$ - $J_3$  model. The AFM  $\Gamma$  interaction has been estimated to be comparable with the  $K$  interaction<sup>36,42,45,50–54</sup>. The AFM  $J_3$  interaction has also been proposed to be as large as the FM  $J$  interaction with its strength being a few times weaker than  $K$  interaction<sup>11,42,48</sup>, or to be much weaker than the NN interactions<sup>37</sup>. Therefore, we clarify the role of the  $\Gamma$  and  $J$  terms in the field-induced phase transition of the  $K$ - $J_3$  model. As shown in Fig. 3(a) [Fig. 3(c)], the multiple-peak structure in the  $a$ -axis field is almost suppressed and a broad (sharp) one-peak structure remains even with a quite small value of  $\Gamma$  ( $J$ ) as large as  $\Gamma/|K| \approx 0.05$  ( $J/|K| \approx -0.15$ ) for  $J_3 = 0.1|K|$ . In the case of the  $c$ -axis field, the first IP determined by peaks  $C_2$  and  $C_3$  collapses when  $\Gamma/|K| \approx 0.04$  ( $J/|K| \approx -0.15$ ). The second IP determined by peaks  $C_3$  and  $C_4$  is robust in the finite  $\Gamma$  ( $J$ ) interaction, although its boundaries shift upward (downward) with the overall IP region shrunk, as shown in Fig. 3(b) [Fig. 3(d)]. This clearly demonstrates why previous models failed to give the IP in the  $a$ -axis field in contrast with the case in the  $c$ -axis field<sup>40,41,43</sup>.

As shown in Fig. 1(d), the IP is clearly distinct from the KSL phase. Moreover, our model hardly identifies the nematic phase proposed as the possible IP of the  $K$ - $\Gamma$ - $\Gamma'$  model<sup>41</sup>. We further verify that the magnetic phase of the classical  $K$ - $J_3$  model continuously varies from the

zigzag order to the fully polarized phase without any IP regardless of the field direction [see Ref. 45 and SM<sup>32</sup>]. Thus, the classical magnetic phase can be ruled out for the IP.

Similar to the  $K$ - $J$  model with AFM  $K$  and FM  $J$  interactions, where  $U(1)$  spin liquid was proposed for the IP<sup>35</sup>, physical quantities such as the spin correlation function and the magnetization in our model calculations show step-like variations around the phase boundaries in the  $c$ -axis field [see SM<sup>32</sup>]. In the field away from the  $c$  axis, the step-like variation is suppressed (not shown here). Such a feature remains in the  $a$ -axis field but entirely diminishes in the  $b$ -axis field. Moreover, the magnetic excitation gap is almost closed at both  $\Gamma$  and  $M$  points, and the excitation spectrum is well-spread like continuum excitations at the  $\Gamma$  point in the vicinity of the IP labeled as ‘IP1’ in Figs. 1(d) and 1(f) [see SM<sup>32</sup>]. This likely implies that the IP1 is possibly  $U(1)$  spin liquid characterized as the gapless fermionic excitation. However, the entanglement entropy calculation of a periodic  $2 \times 16 \times 3$  cluster by the DMRG method reveals that the gap is only closed at the phase boundaries and the IP is gapped [see SM<sup>32</sup>]. Therefore, our DMRG calculation indicates that the gapless  $U(1)$  spin liquid may not be probable as the IP of the  $K$ - $J_3$  model, although the boundaries between the phases are still gapless. Further studies are highly desired to identify the genuine nature of the IP.

*Conclusion* – Based on the numerical calculation with both ED and DMRG methods, we have found that the quantum  $K$ - $J_3$  model can exhibit the magnetic phase transition from the zigzag order phase to the polarized phase via an IP even in the  $a$ -axis field. Our results are in good qualitative agreement with recent observations in the proximate Kitaev material  $\alpha$ - $\text{RuCl}_3$ <sup>28,30,31</sup>. We also found that the IP in the  $a$ -axis field is adiabatically equivalent to the IP in the  $c$ -axis field but diminishes in the  $b$ -axis field. Considering that our model is quite concise, our results provide a new insight on determining a spin Hamiltonian relevant to  $\alpha$ - $\text{RuCl}_3$  and also on understanding its field-induced phase transition.

## ACKNOWLEDGMENTS

*Acknowledgments* – We acknowledge Bongjae Kim, Seung-Hwan Do, Sungdae Ji, Kwang-Yong Choi, Yong-Baek Kim, Hae-Young Kee, Eun-Gook Moon, David A. S. Kaib, and Roser Valentí for fruitful discussion. B.H.K. was supported by KIAS Individual Grants (CG068701). S.S. was supported by Grant-in-Aid for Young Scientists (B) (No. JP17K14148) from MEXT, Japan. S.S. and T.S. were supported by JST PRESTO (No. JPMJPR191B and No. JPMJPR191C), Japan. S.Y. was supported by Grant-in-Aid for Scientific Research (B) (No. JP18H01183) from MEXT, Japan. Y.-W.S. was supported by KIAS Individual Grants (CG031509) and by the NRF of Korea (Grant No. 2017R1A5A1014862,

SRC Program: vdWMRC Center). Numerical computations have been performed with the Center for Advanced

Computation Linux Cluster System at KIAS and the RIKEN supercomputer system (HOKUSAI GreatWave).

- 
- <sup>1</sup> L. Savary and L. Balents, *Rep. Prog. Phys.* **80**, 016502 (2016).
- <sup>2</sup> A. Kitaev, *Ann. Phys.* **321**, 2 (2006).
- <sup>3</sup> S. M. Winter, A. A. Tsirlin, M. Daghofer, J. van den Brink, Y. Singh, P. Gegenwart, and R. Valentí, *J. Phys.: Condens. Matter* **29**, 493002 (2017).
- <sup>4</sup> H. Takagi, T. Takayama, G. Jackeli, G. Khaliullin, and S. E. Nagler, *Nat. Rev. Phys.* **1**, 264 (2019).
- <sup>5</sup> Y. Motome and J. Nasu, *J. Phys. Soc. Jpn.* **89**, 012002 (2020).
- <sup>6</sup> G. Jackeli and G. Khaliullin, *Phys. Rev. Lett.* **102**, 017205 (2009).
- <sup>7</sup> H.-S. Kim, V. S. V., A. Catuneanu, and H.-Y. Kee, *Phys. Rev. B* **91**, 241110(R) (2015).
- <sup>8</sup> Y. Singh and P. Gegenwart, *Phys. Rev. B* **82**, 064412 (2010).
- <sup>9</sup> J. A. Sears, M. Songvilay, K. W. Plumb, J. P. Clancy, Y. Qiu, Y. Zhao, D. Parshall, and Y.-J. Kim, *Phys. Rev. B* **91**, 144420 (2015).
- <sup>10</sup> J. G. Rau, E. K.-H. Lee, and H.-Y. Kee, *Phys. Rev. Lett.* **112**, 077204 (2014).
- <sup>11</sup> S. M. Winter, Y. Li, H. O. Jeschke, and R. Valentí, *Phys. Rev. B* **93**, 214431 (2016).
- <sup>12</sup> B. H. Kim, T. Shirakawa, and S. Yunoki, *Phys. Rev. Lett.* **117**, 187201 (2016).
- <sup>13</sup> L. J. Sandilands, Y. Tian, K. W. Plumb, Y.-J. Kim, and K. S. Burch, *Phys. Rev. Lett.* **114**, 147201 (2015).
- <sup>14</sup> A. Banerjee, C. A. Bridges, J.-Q. Yan, A. A. Aczel, L. Li, M. B. Stone, G. E. Granroth, M. D. Lumsden, Y. Yiu, J. Knolle, S. Bhattacharjee, D. L. Kovrizhin, R. Moessner, D. A. Tennant, D. G. Mandrus, and S. E. Nagler, *Nat. Mater.* **15**, 733 (2016).
- <sup>15</sup> A. Banerjee, J. Yan, J. Knolle, C. A. Bridges, M. B. Stone, M. D. Lumsden, D. G. Mandrus, D. A. Tennant, R. Moessner, and S. E. Nagler, *Science* **356**, 1055 (2017).
- <sup>16</sup> S.-H. Do, S.-Y. Park, J. Yoshitake, J. Nasu, Y. Motome, Y. Kwon, D. T. Adroja, D. J. Voneshen, K. Kim, T.-H. Jang, J.-H. Park, K.-Y. Choi, and S. Ji, *Nat. Phys.* **13**, 1079 (2017).
- <sup>17</sup> S. Widmann, V. Tsurkan, D. A. Prishchenko, V. G. Mazurenko, A. A. Tsirlin, and A. Loidl, *Phys. Rev. B* **99**, 094415 (2019).
- <sup>18</sup> Y. Kubota, H. Tanaka, T. Ono, Y. Narumi, and K. Kindo, *Phys. Rev. B* **91**, 094422 (2015).
- <sup>19</sup> J. A. Sears, Y. Zhao, Z. Xu, J. W. Lynn, and Y.-J. Kim, *Phys. Rev. B* **95**, 180411(R) (2017).
- <sup>20</sup> I. A. Leahy, C. A. Pocs, P. E. Siegfried, D. Graf, S.-H. Do, K.-Y. Choi, B. Normand, and M. Lee, *Phys. Rev. Lett.* **118**, 187203 (2017).
- <sup>21</sup> S.-H. Baek, S.-H. Do, K.-Y. Choi, Y. S. Kwon, A. U. B. Wolter, S. Nishimoto, J. van den Brink, and B. Büchner, *Phys. Rev. Lett.* **119**, 037201 (2017).
- <sup>22</sup> Z. Wang, S. Reschke, D. Hüvonen, S.-H. Do, K.-Y. Choi, M. Gensch, U. Nagel, T. Rööm, and A. Loidl, *Phys. Rev. Lett.* **119**, 227202 (2017).
- <sup>23</sup> J. Zheng, K. Ran, T. Li, J. Wang, P. Wang, B. Liu, Z.-X. Liu, B. Normand, J. Wen, and W. Yu, *Phys. Rev. Lett.* **119**, 227208 (2017).
- <sup>24</sup> A. U. B. Wolter, L. T. Corredor, L. Janssen, K. Nenkov, S. Schönecker, S.-H. Do, K.-Y. Choi, R. Albrecht, J. Hunger, T. Doert, M. Vojta, and B. Büchner, *Phys. Rev. B* **96**, 041405(R) (2017).
- <sup>25</sup> A. Banerjee, P. Lampen-Kelley, J. Knolle, C. Balz, A. A. Aczel, B. Winn, Y. Liu, D. Pajerowski, J. Yan, C. A. Bridges, A. T. Savici, B. C. Chakoumakos, M. D. Lumsden, D. A. Tennant, R. Moessner, D. G. Mandrus, and S. E. Nagler, *npj Quantum Materials* **3**, 8 (2018).
- <sup>26</sup> Y. Kasahara, T. Ohnishi, Y. Mizukami, O. Tanaka, S. Ma, K. Sugii, N. Kurita, H. Tanaka, J. Nasu, Y. Motome, T. Shibauchi, and Y. Matsuda, *Nature* **559**, 227 (2018).
- <sup>27</sup> N. Janša, A. Zorko, M. Gomilšek, M. Pregelj, K. W. Krämer, D. Biner, A. Biffin, C. Rüegg, and M. Klanjšek, *Nat. Phys.* **14**, 786 (2018).
- <sup>28</sup> P. Lampen-Kelley, L. Janssen, E. C. Andrade, S. Rachel, J.-Q. Yan, C. Balz, D. G. Mandrus, S. E. Nagler, and M. Vojta, [arXiv:1807.06192](https://arxiv.org/abs/1807.06192).
- <sup>29</sup> C. Wellm, J. Zeisner, A. Alfonsov, A. U. B. Wolter, M. Roslova, A. Isaeva, T. Doert, M. Vojta, B. Büchner, and V. Kataev, *Phys. Rev. B*, 184408 (2018).
- <sup>30</sup> C. Balz, P. Lampen-Kelley, A. Banerjee, J. Yan, Z. Lu, X. Hu, S. M. Yadav, Y. Takano, Y. Liu, D. A. Tennant, M. D. Lumsden, D. Mandrus, and S. E. Nagler, *Phys. Rev. B* **100**, 060405(R) (2019).
- <sup>31</sup> T. Yokoi, S. Ma, Y. Kasahara, S. Kasahara, T. Shibauchi, N. Kurita, H. Tanaka, J. Nasu, Y. Motome, C. Hickey, S. Trebst, and Y. Matsuda, [arXiv:2001.01899](https://arxiv.org/abs/2001.01899).
- <sup>32</sup> See Supplemental Material for the detail on the ED and DMRG calculations, analysis of the zigzag order phase in the low-field limit, the cluster geometry dependency of the ED calculation, results for the classical  $K$ - $J_3$  model, results of static spin correlation, magnetization, and dynamical spin correlation, and results of the entanglement entropy behaviors.
- <sup>33</sup> S. Agrestini, C.-Y. Kuo, K.-T. Ko, Z. Hu, D. Kasinathan, H. B. Vasili, J. Herrero-Martin, S. M. Valvidares, E. Pellegrin, L.-Y. Jang, A. Henschel, M. Schmidt, A. Tanaka, and L. H. Tjeng, *Phys. Rev. B* **96**, 161107(R) (2017).
- <sup>34</sup> R. Yadav, N. A. Bogdanov, V. M. Katukuri, S. Nishimoto, J. van den Brink, and L. Hozoi, *Sci. Rep.* **6**, 37925 (2016).
- <sup>35</sup> Y.-F. Jiang, T. P. Devereaux, and H.-C. Jiang, *Phys. Rev. B* **100**, 165123 (2019).
- <sup>36</sup> K. Ran, J. Wang, W. Wang, Z.-Y. Dong, X. Ren, S. Bao, S. Li, Z. Ma, Y. Gan, Y. Zhang, J. T. Park, G. Deng, S. Danilkin, S.-L. Yu, J.-X. Li, and J. Wen, *Phys. Rev. Lett.* **118**, 107203 (2017).
- <sup>37</sup> W. Wang, Z.-Y. Dong, S.-L. Yu, and J.-X. Li, *Phys. Rev. B* **96**, 115103 (2017).
- <sup>38</sup> M. Gohlke, G. Wachtel, Y. Yamaji, F. Pollmann, and Y. B. Kim, *Phys. Rev. B* **97**, 075126 (2018).
- <sup>39</sup> A. Catuneanu, Y. Yamaji, G. Wachtel, Y. B. Kim, and H.-Y. Kee, *npj Quantum Materials* **3**, 23 (2018).
- <sup>40</sup> J. S. Gordon, A. Catuneanu, E. S. Sørensen, and H.-Y. Kee, *Nat. Commun.* **10**, 2470 (2019).
- <sup>41</sup> H.-Y. Lee, R. Kaneko, L. E. Chern, T. Okubo,

- Y. Yamaji, N. Kawashima, and Y. B. Kim, *Nat. Commun.* **11**, 1639 (2020).
- <sup>42</sup> S. M. Winter, K. Riedl, P. A. Maksimov, A. L. Chernyshev, A. Honecker, and R. Valentí, *Nat. Commun.* **8**, 1152 (2017).
- <sup>43</sup> S. M. Winter, K. Riedl, D. Kaib, R. Coldea, and R. Valentí, *Phys. Rev. Lett.* **120**, 077203 (2018).
- <sup>44</sup> Y. S. Hou, H. J. Xiang, and X. G. Gong, *Phys. Rev. B* **96**, 054410 (2017).
- <sup>45</sup> L. Janssen, E. C. Andrade, and M. Vojta, *Phys. Rev. B* **96**, 064430 (2017).
- <sup>46</sup> C. Eichstaedt, Y. Zhang, P. Laurell, S. Okamoto, A. G. Eguiluz, and T. Berlijn, *Phys. Rev. B* **100**, 075110 (2019).
- <sup>47</sup> P. Laurell and S. Okamoto, *npj Quantum Materials* **5**, 2 (2020).
- <sup>48</sup> P. A. Maksimov and A. L. Chernyshev, *Phys. Rev. Res.* **2**, 033011 (2020).
- <sup>49</sup> C. Hickey and S. Trebst, *Nat. Commun.* **10**, 530 (2019).
- <sup>50</sup> J. A. Sears, L. E. Chern, S. Kim, P. J. Bereciartua, S. Francoual, Y. B. Kim, and Y.-J. Kim, *Nat. Phys.* **16**, 837 (2020).
- <sup>51</sup> J. Chaloupka and G. Khaliullin, *Phys. Rev. B* **94**, 064435 (2016).
- <sup>52</sup> L. Wu, A. Little, E. E. Aldape, D. Rees, E. Thewalt, P. Lampen-Kelley, A. Banerjee, C. A. Bridges, J.-Q. Yan, D. Boone, S. Patankar, D. Goldhaber-Gordon, D. Mandrus, S. E. Nagler, E. Altman, and J. Orenstein, *Phys. Rev. B* **98**, 094425 (2018).
- <sup>53</sup> P. Lampen-Kelley, S. Rachel, J. Reuther, J.-Q. Yan, A. Banerjee, C. A. Bridges, H. B. Cao, S. E. Nagler, and D. Mandrus, *Phys. Rev. B* **98**, 100403(R) (2018).
- <sup>54</sup> I. O. Ozel, C. A. Belvin, E. Baldini, I. Kimchi, S. Do, K.-Y. Choi, and N. Gedik, *Phys. Rev. B* **100**, 085108 (2019).

# Supplemental Material: Proximate Kitaev system for an intermediate magnetic phase in in-plane magnetic fields

Beom Hyun Kim,<sup>1</sup> Shigetoshi Sota,<sup>2</sup> Tomonori Shirakawa,<sup>2</sup> and Seiji Yunoki,<sup>2,3,4</sup> and Young-Woo Son<sup>1</sup>

<sup>1</sup>*Korea Institute for Advanced Study, Seoul 02455, South Korea*

<sup>2</sup>*Computational Materials Science Research Team, RIKEN Center for Computational Science (R-CCS), Kobe, Hyogo 650-0047, Japan*

<sup>3</sup>*Computational Condensed Matter Physics Laboratory, RIKEN Cluster for Pioneering Research (CPR), Saitama 351-0198, Japan*

<sup>4</sup>*Computational Quantum Matter Research Team, RIKEN, Center for Emergent Matter Science (CEMS), Wako, Saitama 351-0198, Japan*

## S1. ED CALCULATION

To explore the ground state magnetic phase of the  $K$ - $J_3$  model, we adopt a periodic 24-site cluster shown in Fig. S1(b), which is invariant under the  $C_3$  rotation along the  $c$  axis. Using the exact diagonalization (ED) method based on the Lanczos algorithm, we calculate the ground state and its energy. In the pure Kitaev model ( $J_3 = 0$ ), the ground state is the Kitaev spin liquid (KSL) and the expectation value of the plaquette operator  $W_p = 2^6 S_{1x} S_{2y} S_{3z} S_{4x} S_{5y} S_{6z}$  for one hexagon [see Fig. S1(b)] should be exactly one. The static spin correlation (SC) function  $\langle \mathbf{S}_{-\mathbf{q}} \cdot \mathbf{S}_{\mathbf{q}} \rangle$  does not show any peak structure at specific momentum  $\mathbf{q}$  due to the quantum paramagnetism. Here,  $\mathbf{S}_{\mathbf{q}} = \frac{1}{\sqrt{N}} \sum_{i=1}^N e^{-i\mathbf{q} \cdot \mathbf{r}_i} \mathbf{S}_i$ ,  $\mathbf{r}_i$  is the spatial location of the  $i$ th spin  $\mathbf{S}_i$  in the honeycomb lattice [see Fig. S1(b)], and  $N$  is the number of sites. When  $J_3$  is turned on, the ground state changes from the pure KSL phase. Until the critical value of  $J_3$ , however, it is still adiabatically connected to the KSL phase even though  $\langle W_p \rangle$  slightly deviates from one. When the magnitude of  $J_3$  is larger than the critical value ( $J_3/|K| \approx 0.033$ ),  $\langle W_p \rangle$  is suddenly dropped and slowly saturated down to a negative value ( $\approx -0.19$ ) when  $J_3/|K| > 0$ . Concomitantly,  $\langle \mathbf{S}_{-\mathbf{q}} \cdot \mathbf{S}_{\mathbf{q}} \rangle$  at the  $M$  points abruptly jumps. This supports that the magnetic ground state changes from the KSL phase to the zigzag order phase [see Fig. S1(c) and S1(d)].

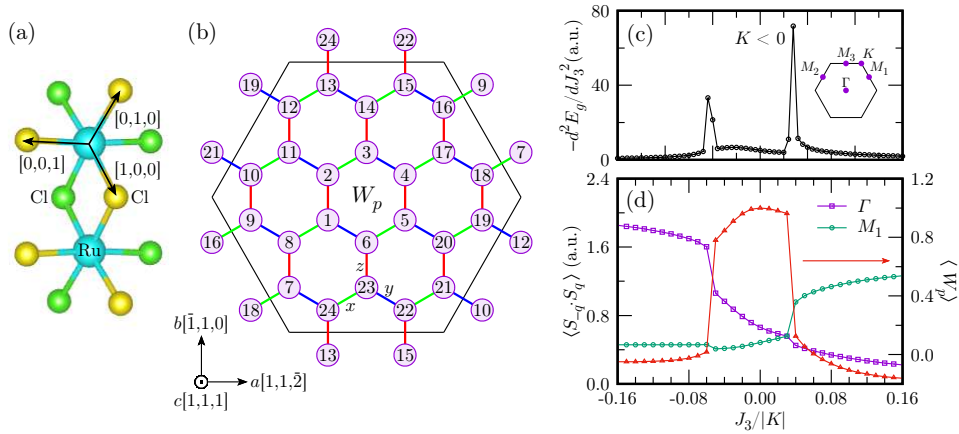


FIG. S1. (a) Schematic diagram of two Ru ions mediated via edge-sharing Cl ions along the  $b$  axis in  $\alpha$ - $\text{RuCl}_3$ . Cyan balls refer to Ru ions, and yellow and green balls represent Cl ions above and below the  $ab$  plane, respectively. Black arrows denote local coordinate axes  $[1,0,0]$ ,  $[0,1,0]$ , and  $[0,0,1]$  pointing from the central Ru ion to the upper Cl ions in a  $\text{RuCl}_6$  octahedron, which represent the local coordinates of spin  $\mathbf{S}_i = (S_{ix}, S_{iy}, S_{iz})$ . (b) Schematic diagram of a periodic 24-site cluster. Green, blue, and red lines refer to  $x$ -,  $y$ -, and  $z$ -type neighboring bonds, respectively. Six sites in the central hexagon are used to calculate the expectation value of plaquette operator ( $W_p$ ). Lattice coordinates ( $a$ ,  $b$ , and  $b$  axes) are also indicated as  $[1,1,2]$ ,  $[\bar{1},1,0]$ , and  $[1,1,1]$  in terms of the local coordinates of spins. (c) Second derivative of the ground state energy ( $-d^2 E_g / dJ_3^2$ ) with respect to the third nearest neighboring interaction  $J_3$  and (d) static spin correlation functions  $\langle \mathbf{S}_{-\mathbf{q}} \cdot \mathbf{S}_{\mathbf{q}} \rangle$  at the  $\Gamma$  and  $M_1$  points, and the expectation value of the plaquette operator  $W_p$  as a function of  $J_3$  for the  $K$ - $J_3$  model with the ferromagnetic Kitaev interaction ( $K < 0$ ) calculated on the periodic 24-site cluster using the ED method. Brillouin zone of a honeycomb lattice is also shown in the inset of (c).

## S2. ANALYSIS OF THE ZIGZAG ORDER PHASE IN THE LOW-FIELD LIMIT

To explore the zigzag order phase more carefully, we examine the evolution of three lowest excited states with the  $a$ -axis field at  $J_3/|K| = 0.1$ . As shown in Fig. S2(a), the excitation energy of the first excited state is much smaller than those of the second and third excited states in the low-field limit. When the magnetic field is within the region bounded by peaks  $A_1$  and  $A_2$  of  $-d^2E_g/dh^2$  at  $\mu_B h/|K| \approx 0.03$  and  $0.05$ , respectively [also see Fig. 1(b) in the main text], the first excitation energy becomes almost zero. Also,  $|\langle \Psi_g(h) | \Psi_g(0) \rangle|^2$  and  $|\langle \Psi_g(h) | \Psi_1(0) \rangle|^2$  show the hollow and hump, respectively, in this region [see Fig. S2(b)]. It implies that the ground and first excited states in the zero field are certainly mixed together in this region, thus leading to the abrupt change of the ground and first excited states at the fields corresponding to peaks  $A_1$  and  $A_2$ . Note that the ground and first excited states both show dominant intensity of the static SC function  $\langle \mathbf{S}_{-\mathbf{q}} \cdot \mathbf{S}_{\mathbf{q}} \rangle$  at the  $M$  points up to the magnetic field corresponding to peak  $A_3$  [see Fig. S2(c) and S2(d)]. Therefore, it hardly involves any genuine phase transition in this region. Similarly, from the results shown in Fig. S2(e) and S2(f), we can conclude that peaks  $B_1$  and  $C_1$  of  $-d^2E_g/dh^2$  in the  $b$ - and  $c$ -axis fields [see Figs. 1(b) and 1(c) in the main text] are not related to a phase transition, either.

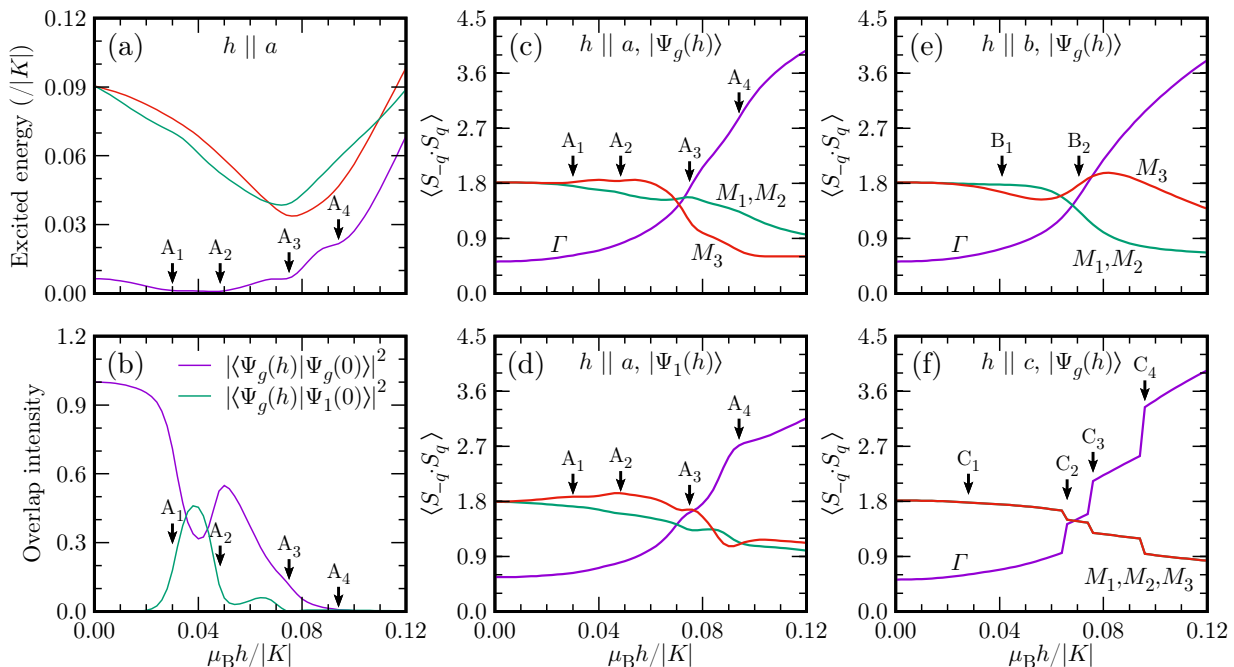


FIG. S2. (a) Evolution of the three lowest excitation energies with the  $a$ -axis field  $h$ . (b) The overlap intensity among the ground and first excited states,  $|\Psi_g(h)\rangle$  and  $|\Psi_1(h)\rangle$ , respectively, in the magnetic field  $h$  along the  $a$  axis. (c)–(f) Static spin correlation function  $\langle \mathbf{S}_{-\mathbf{q}} \cdot \mathbf{S}_{\mathbf{q}} \rangle$  at the  $M_1$ ,  $M_2$ ,  $M_3$ , and  $\Gamma$  points for the ground states  $|\Psi_g(h)\rangle$  in the  $a$ -,  $b$ - and  $c$ -axis fields, and the first excited state  $|\Psi_1(h)\rangle$  in the  $a$ -axis field. Arrows indicate the positions of peaks  $A_{1-4}$ ,  $B_{1,2}$ , and  $C_{1-4}$  of  $-d^2E_g/dh^2$  [see Figs. 1(b) and 1(c) in the main text]. All results are obtained for the  $K$ - $J_3$  model with the ferromagnetic Kitaev interaction ( $K < 0$ ) and  $J_3/|K| = 0.1$  calculated on a periodic 24-site cluster using the ED method.

## S3. CLUSTER GEOMETRY DEPENDENCE

To check the cluster geometry dependence on the magnetic phase transition of the  $K$ - $J_3$  model in the magnetic field, here we perform the ED calculation on a periodic  $2 \times 4 \times 3$  cluster [for the geometry of the cluster, see Fig. S4(a)]. Unlike the 24-site cluster shown in Fig. S1(b), the  $2 \times 4 \times 3$  cluster does not have the  $C_3$  rotation symmetry. Instead, it is invariant under the  $C_2$  rotation. Figure S3 shows the results of  $-d^2E_g/dh^2$  in the  $a$ -,  $b$ -, and  $c$ -axis fields for  $J_3/|K| = 0.1$ , which are also compared with those for the  $C_3$  rotationally symmetric 24-site cluster. Because these clusters are still too small to avoid the finite size effect, the field dependence of  $-d^2E_g/dh^2$  evidently depends on the cluster geometry. Nevertheless, the overall shapes are consistent with each other except that there are two peaks in the  $2 \times 4 \times 3$  cluster, while there are three peaks in the  $C_3$  rotationally symmetric 24-site cluster, in the large  $c$ -axis field  $\mu_B h/|K| > 0.05$ . The emergence of the intermediate phase (IP) in the  $a$ - and  $c$ -axis fields, and the absence of

any IP in the  $b$ -axis field are identified in both clusters. However, the number of consecutive IPs is hardly determined. It depends strongly on the geometry and size of clusters.

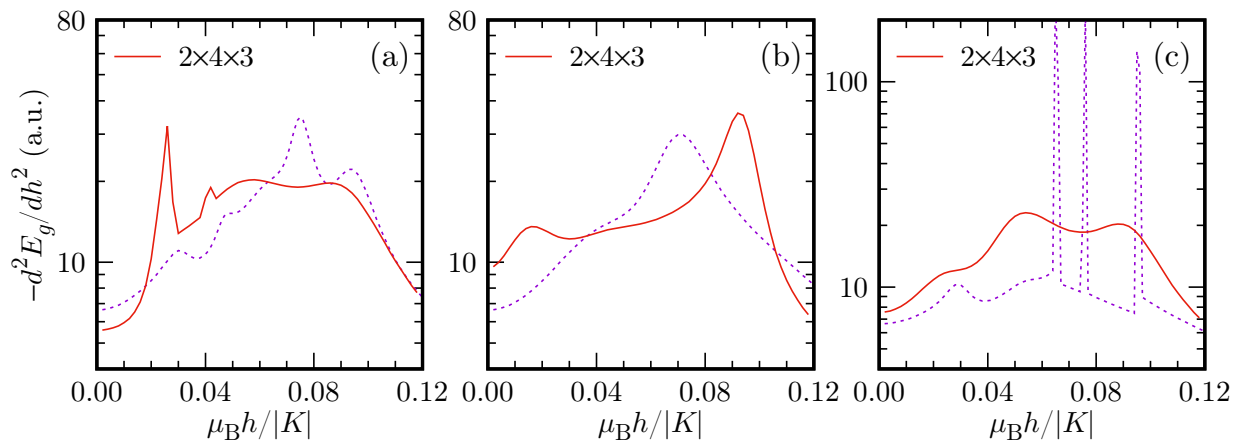


FIG. S3. Second derivative of the ground state energy ( $d^2 E_g / dh^2$ ) with respect to the magnetic field  $h$  along (a) the  $a$  axis, (b) the  $b$  axis, and (c) the  $c$  axis for the periodic  $2 \times 4 \times 3$  cluster. Schematic diagram of the periodic  $2 \times L_1 \times L_2$  cluster is shown in Fig. S4(a). For comparison, the results for the  $C_3$  rotationally symmetric 24-site cluster is also shown by dotted lines. All results are obtained for the  $K$ - $J_3$  model with  $K < 0$  and  $J_3/|K| = 0.1$  calculated using the ED method.

#### S4. DMRG CALCULATION

To solve the  $K$ - $J_3$  model with the density matrix renormalization group (DMRG) method, we consider a periodic  $2 \times 4 \times 4$  cluster shown in Fig. S4(a). To verify the relevance of the DMRG calculation in the two-dimensional  $K$ - $J_3$  model, we also perform the DMRG calculation of a periodic  $2 \times 4 \times 3$  cluster and compare it with the ED calculation. Figure S4(b) shows the energies calculated by the ED and DMRG methods for various values of the  $a$ -axis field when we keep up to  $m = 2000$  eigenstates with largest eigenvalues of the reduced density matrix of the ground state in the DMRG calculation. We check that the energy is converged with the accuracy less than  $10^{-7}|K|$ . Despite of the two-dimensional system, the DMRG calculation is thus adequate to obtain the ground state of the  $K$ - $J_3$  model. In the case of the periodic  $2 \times 4 \times 4$  cluster, we increase the number of density-matrix eigenstates kept up to  $m = 2500$  for better convergence. Because of the large computational cost, we perform the calculation with a mild truncation error of the ground state energy around  $10^{-7}|K| \sim 10^{-4}|K|$ .

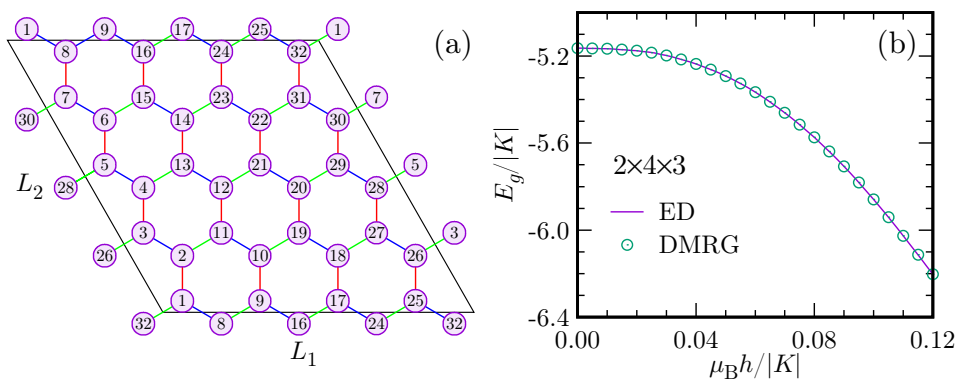


FIG. S4. (a) Schematic diagram of a periodic  $2 \times L_1 \times L_2$  cluster with  $L_1 = L_2 = 4$ . (b) Ground state energy  $E_g$  as a function of the magnetic field  $h$  along the  $a$  axis for the  $K$ - $J_3$  model with the ferromagnetic Kitaev interaction ( $K < 0$ ) and  $J_3/|K| = 0.1$  calculated on a periodic  $2 \times 4 \times 3$  cluster using the ED and DMRG methods.

## S5. CLASSICAL MONTE-CARLO CALCULATION

To understand the magnetic phase transition of the classical  $K$ - $J_3$  model in the presence of the magnetic field, we consider a periodic  $2 \times 24 \times 24$  cluster [for the geometry of the cluster, see Fig. S4(a)] and perform the classical Monte-Carlo (MC) calculation with the standard Metropolis algorithm. Figure S5 shows the evolution of order parameters  $O_\Gamma$  and  $O_M$  (i.e. static SC function  $\langle \mathbf{S}_{-\mathbf{q}} \cdot \mathbf{S}_{\mathbf{q}} \rangle$  at the  $\Gamma$  and  $M$  points, respectively) for the polarized phase and the zigzag order phase for  $J_3/|K| = 0.1$  at temperature  $k_B T/|K| = 0.01$  in the  $a$ - and  $c$ -axis fields calculated with 40000 MC steps after 20000 MC steps for thermalization. As the magnetic field increases, the order parameter for the zigzag order phase decreases with increasing the slop until losing all intensity, while that for the polarized phase almost linearly increases until it is completely saturated. No indication of an intermediate phase is observed during the phase transition from the zigzag order phase to the polarized phase.

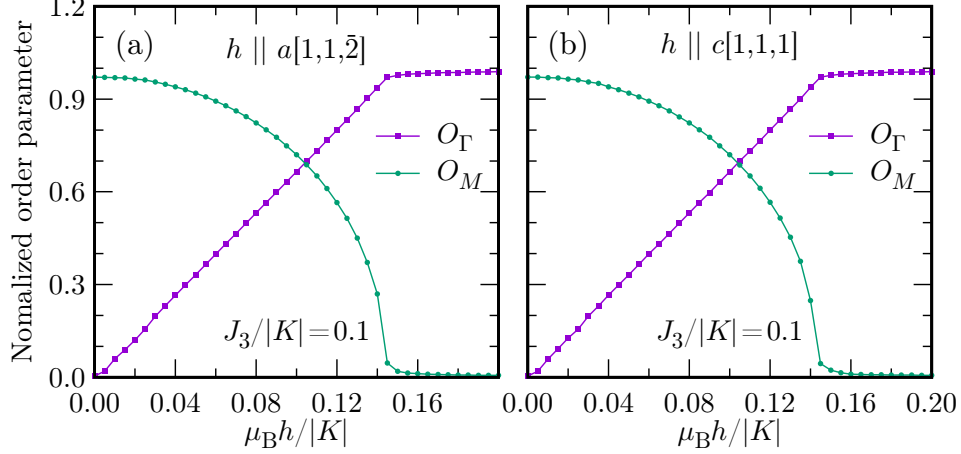


FIG. S5. Evolution of order parameters for the zigzag order phase ( $O_M$ ) and the polarized phase ( $O_\Gamma$ ) as a function of the external magnetic field along (a) the  $a$  axis and (b) the  $c$  axis for the classical  $K$ - $J_3$  model with  $J_3/|K| = 0.1$ . The temperature is set to be  $0.01|K|/k_B$  and a periodic  $2 \times 24 \times 24$  cluster is used in the classical MC calculation.

## S6. STATIC SPIN CORRELATION, MAGNETIZATION, AND DYNAMICAL SPIN CORRELATION

To gain an insight on the IP, we calculate the static SC functions  $\langle \mathbf{S}_i \cdot \mathbf{S}_j \rangle$ , magnetizations, and dynamical SC functions for the  $K$ - $J_3$  model on the periodic 24-site cluster shown in Fig. S1(a) in the presence of the magnetic field.

Figures S6(a)–S6(c) show the static SC functions in the  $a$ -,  $b$ -, and  $c$ -axis fields. In the case of  $J_3/|K| = 0.1$  with no magnetic field where the zigzag order is dominant, strong FM Kitaev and AFM  $J_3$  interactions lead to positive SC function ( $\approx 0.12$ ) among nearest neighboring (NN) spins and negative SC function ( $\approx -0.24$ ) among third NN spins. On the other hand, the SC function among second NN spins is as large as  $-0.068$ . This is because two spins at second NN sites can simultaneously belong to only one of the three FM zigzag chains determined by the ordering momenta,  $M_1$ ,  $M_2$ , and  $M_3$  points. Thus, the SC function among second NN spins is the average value of two AFM and one FM correlations.

When the magnetic field is weak enough ( $\mu_B h/|K| \lesssim 0.06$ ), the zigzag order is still dominant and the static SC functions are almost robust [see Figs. S6(a)–S6(c)]. In the  $c$ -axis field, two consecutive IPs take place with increasing the field. As shown in Fig. S6(c), all SC functions vary discontinuously at the boundaries of the IPs. With further increasing the field, the SC functions eventually become all positive because all spins are almost polarized along the field direction. In the  $a$ -axis field, the discontinuous change of the SC functions is somewhat suppressed but the steep variation of the SC functions still appears around the IP boundaries and their slope becomes slightly moderate in the IP region [see Fig. S6(a)]. In contrast, in the  $b$ -axis field, the SC functions change abruptly around the critical field and then increase continuously, as shown in Fig. S6(b).

Figures S6(d)–S6(f) show the magnetization per site along the respective field direction as a function of the magnetic field along the  $a$ ,  $b$ , and  $c$  axes. In the  $c$ -axis field, the step-like magnetization is manifested around the IPs. This is reminiscence of the magnetization plateau frequently observed in frustrated quantum magnets. When the field is applied away from the  $c$  axis, the step-like feature becomes diminished. However, we can still notice that the slope of

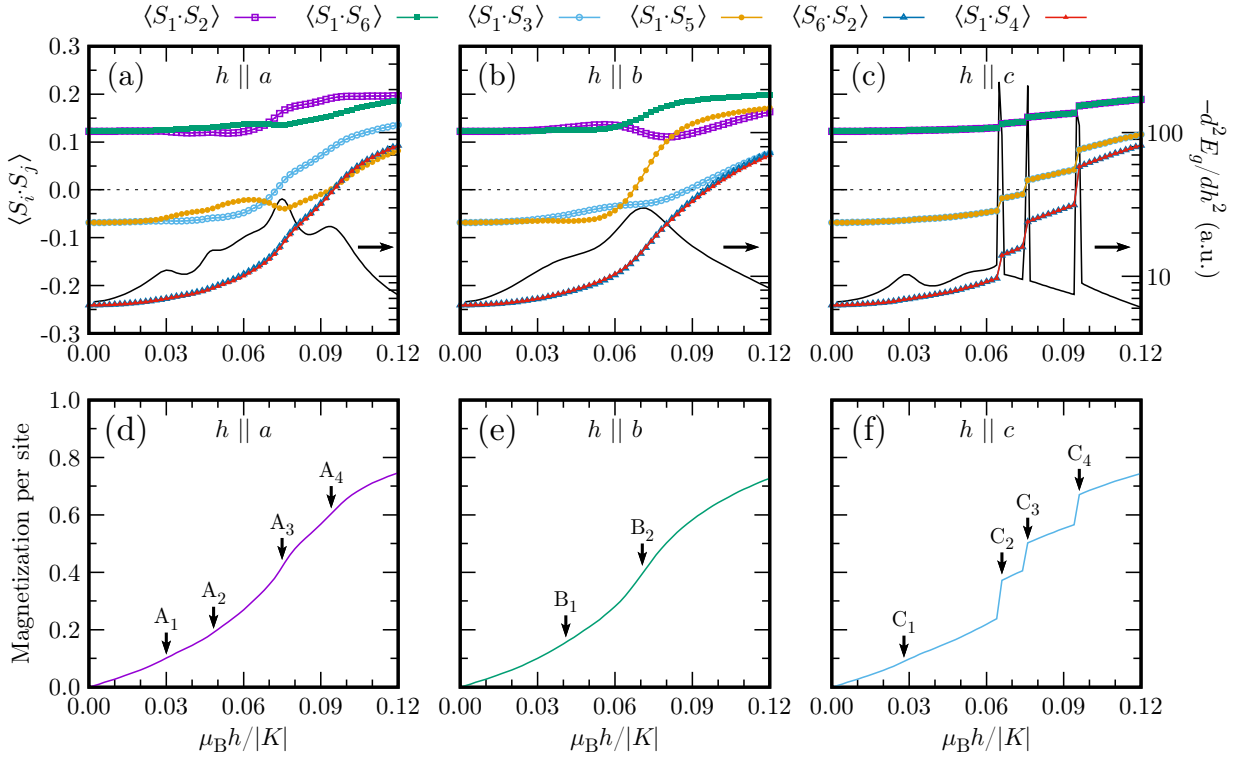


FIG. S6. (a)–(c) Spin correlation functions  $\langle \mathbf{S}_i \cdot \mathbf{S}_j \rangle$  between NN spins ( $\langle \mathbf{S}_1 \cdot \mathbf{S}_2 \rangle$ ,  $\langle \mathbf{S}_1 \cdot \mathbf{S}_6 \rangle$ ), second NN spins ( $\langle \mathbf{S}_1 \cdot \mathbf{S}_3 \rangle$ ,  $\langle \mathbf{S}_1 \cdot \mathbf{S}_5 \rangle$ ), and third NN spins ( $\langle \mathbf{S}_6 \cdot \mathbf{S}_3 \rangle$ ,  $\langle \mathbf{S}_1 \cdot \mathbf{S}_4 \rangle$ ) as a function of the magnetic field  $h$  along (a) the  $a$  axis, (b) the  $b$  axis, and (c) the  $c$  axis. The locus of spins in the cluster are indicated in Fig. S1(a). (d)–(f) Magnetization per site along the field direction as a function of the magnetic field  $h$  along (d) the  $a$  axis, (e) the  $b$  axis, and (f) the  $c$  axis. For comparison, second derivative of the ground state energy ( $d^2 E_g / dh^2$ ) with respect to the field is also shown in (a)–(c). Arrows in (d)–(f) indicate the positions of peaks  $A_{1-4}$ ,  $B_{1,2}$ , and  $C_{1-4}$  of  $-d^2 E_g / dh^2$  [also see Figs. 1(b) and 1(c) in the main text]. All results are obtained for the  $K$ - $J_3$  model with the ferromagnetic Kitaev interaction ( $K < 0$ ) and  $J_3 / |K| = 0.1$  calculated on a periodic 24-site cluster using the ED method.

the magnetization curve changes somewhat discontinuously around the boundaries of the IP in the  $a$ -axis field, while the magnetization simply increases smoothly in the  $b$ -axis field.

Dynamical SC function  $C_{\mathbf{q}}(\omega)$  at momentum  $\mathbf{q}$  and energy  $\omega$  is given as

$$C_{\mathbf{q}}(\omega) = -\frac{1}{\pi} \text{Im} \left[ \sum_{a \in \{x, y, z\}} \left\langle S_{-\mathbf{q}, a} \frac{1}{\omega - H + E_g + i\delta} S_{\mathbf{q}, a} \right\rangle \right], \quad (\text{S1})$$

where  $E_g$  is the ground state energy and  $\delta (= 0.025|K|)$  is the broadening parameter. Figure S7 shows  $C_{\Gamma}(\omega)$ ,  $C_{M_1}(\omega)$ , and  $C_{M_3}(\omega)$  for the  $K$ - $J_3$  model in the  $a$ -,  $b$ -, and  $c$ -axis fields. Note that  $C_{M_2}(\omega)$  is exactly the same as  $C_{M_1}(\omega)$  in these three magnetic fields due to the symmetry.

As shown in Figs. S7(a)–S7(c),  $C_{\Gamma}(\omega)$  exhibits strong spectral weight at  $\omega / |K| \approx 0.25$  when  $h = 0$ , determining the excitation gap in the absence of the field. Applying the magnetic field, the spectral weight is spread over a wide region of  $\omega$  in any field direction. The excitation gap is decreased with increasing the field until the zigzag order phase is no longer robust. The excitation gaps are about  $0.038|K|$ ,  $0.045|K|$ , and  $0.046|K|$  at the phase boundaries corresponding to the  $A_3$  position ( $\mu_B h / |K| \approx 0.075$ ),  $B_2$  position ( $\mu_B h / |K| \approx 0.071$ ), and  $C_2$  position ( $\mu_B h / |K| \approx 0.066$ ) in the  $a$ -,  $b$ -, and  $c$ -axis fields, respectively. In the  $b$ -axis field, the excitation gap begins to increase with further increasing the field above the  $B_2$  position. In the  $a$ -axis field, the excitation gap similarly increases after the  $A_3$  position except that a weak spectral weight arises below the main excitation spectra [see Fig. S7(a)]. In the  $c$ -axis field, the excitation spectra change discontinuously around the phase boundaries, similar to the evolution of the static SC function and the magnetization shown in Figs. S6(c) and S6(f), respectively. The excitation gap suddenly drops from  $0.046|K|$  to zero at the  $C_2$  position and then simply increases with further increasing the field. Notice also that as in the case of the  $a$ -axis field, a weak spectral weight arises below the main spectral weight. The excitation gap detected from this emergent weak spectral weight closes at the phase boundaries determined by the  $C_3$  position ( $\mu_B h / |K| \approx 0.076$ ) and

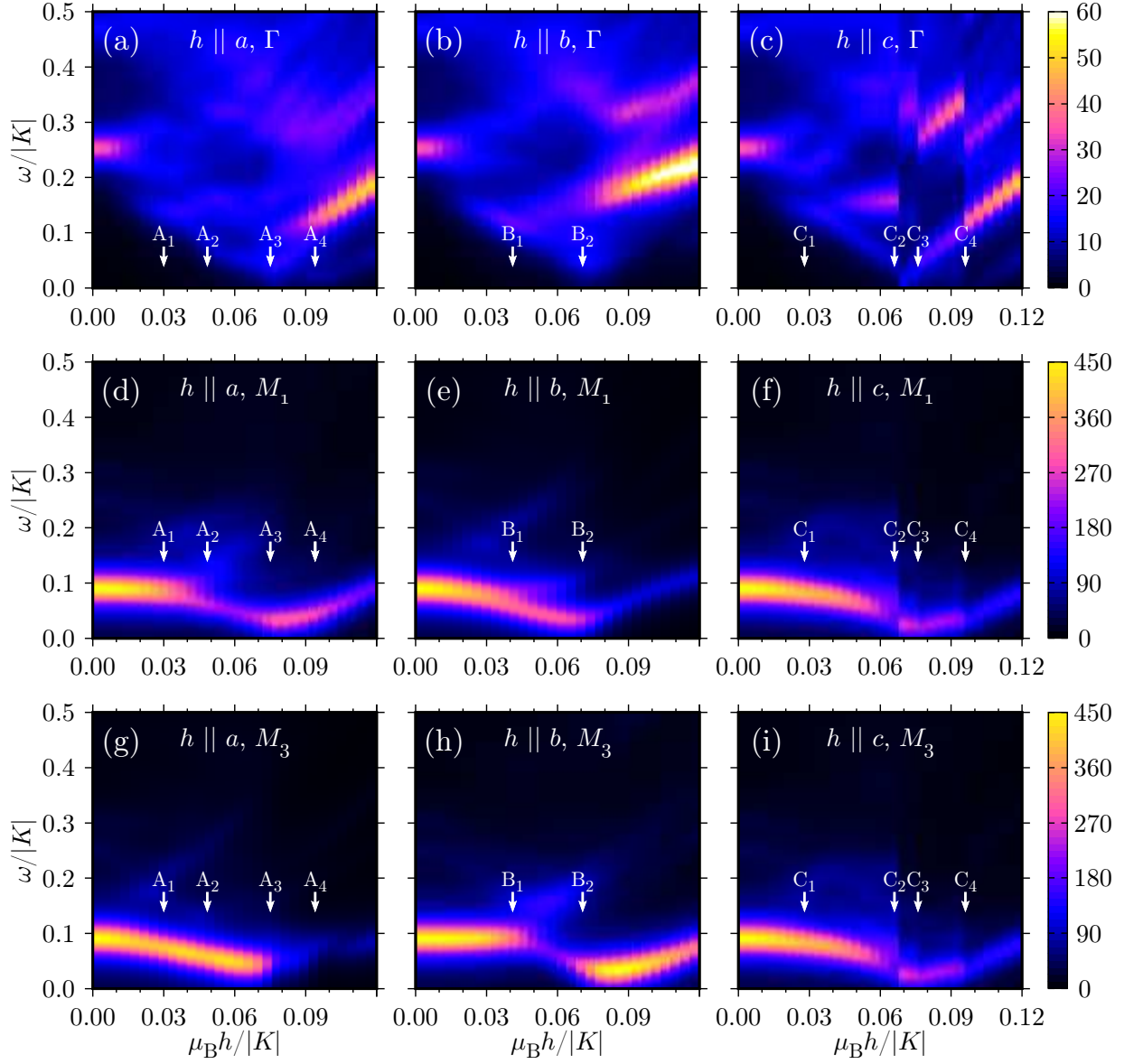


FIG. S7. Dynamical spin correlation functions  $C_{\mathbf{q}}(\omega)$  as a function of the magnetic field  $h$  along the  $a$  axis at (a) the  $\Gamma$  point, (d) the  $M_1$  point, and (g) the  $M_3$  point, along the  $b$  axis at (b) the  $\Gamma$  point, (e) the  $M_1$  point, and (h) the  $M_3$  point, and along the  $c$  axis at (c) the  $\Gamma$  point, (f) the  $M_1$  point, and (i) the  $M_3$  point. White arrows indicate the positions of peaks  $A_{1-4}$ ,  $B_{1,2}$ , and  $C_{1-4}$  of  $-d^2 E_g/dh^2$  [see Fig. 1(b) and 1(c) in the main text]. For clarity, the elastic contribution of  $C_{\mathbf{q}}(\omega)$  at  $\omega = 0$  is omitted. All results are obtained for the  $K$ - $J_3$  model with the ferromagnetic Kitaev interaction ( $K < 0$ ) and  $J_3/|K| = 0.1$  calculated on a periodic 24-site cluster using the ED method.

$C_4$  position ( $\mu_B h/|K| \approx 0.096$ ), and increases monotonically in the polarized phase.

As shown in Figs. S7(d)–S7(i),  $C_{M_1}(\omega)$  and  $C_{M_3}(\omega)$  show strong spectral weight at  $\omega/|K| \approx 0.09$  in the absence of the field. In contrast with  $C_{\Gamma}(\omega)$ , these spectral weights are hardly spread even in the finite fields when the zigzag order is stabilized. In the  $a$ -axis field,  $C_{M_1}(\omega)$  has a minimum excitation gap ( $\approx 0.025|K|$ ) around the phase boundary between the zigzag order phase and the IP. In the  $b$ -axis field,  $C_{M_3}(\omega)$  has a minimum excitation gap ( $\approx 0.033|K|$ ) at  $\mu_B h/|K| \approx 0.08$ , which is slightly larger than the critical field  $\mu_B h/|K| \approx 0.071$  ( $B_2$  position). In the  $c$ -axis field, the minimum excitation gap ( $\approx 0.022|K|$ ) of  $C_{M_1}(\omega)$  and  $C_{M_3}(\omega)$  appears at  $\mu_B h/|K| \approx 0.076$ , the phase boundary between the two IPs ( $C_3$  position). Inside these two IPs, the variation of the excitation gap is not much strong.

## S7. ENTANGLEMENT ENTROPY BEHAVIORS

To further investigate the characteristic feature of the IP, we explore the entanglement entropy (EE) of the  $K$ - $J_3$  model on a periodic  $2 \times L_1 \times L_2$  cluster with  $L_1 = 16$  and  $L_2 = 3$  by the DMRG method keeping  $m = 1500$  (see Sec. S4). We calculate the von Neumann entanglement entropy of the subsystem by varying the subsystem length  $l_1$  from  $l_1 = 1$  to  $L_1/2$  along the  $L_1$  direction, i.e.,

$$S(l_1, L_1) = -\text{Tr}_{l_1} \rho_{l_1} \ln \rho_{l_1}, \quad (\text{S2})$$

where  $\text{Tr}_{l_1}$  is the trace over all basis on the subsystem and  $\rho_{l_1}$  is the reduced density matrix of the subsystem. Figure S8(a) shows  $S(l_1, L_1)$  for various  $c$ -axis field strengths ( $\mu_B h/|K| = 0.05, 0.055, 0.07, 0.08, 0.09, 0.095, \text{ and } 0.1$ ) when  $J_3/|K| = 0.1$ . The calculated EEs for  $l_1 > 2$  can be fitted reasonably well with the prediction of the conformal field theory (CFT) for a 1 + 1 dimensional critical system, i.e.,

$$S(l_1, L_1) = \frac{c}{3} \ln \left[ \frac{L_1}{\pi} \sin \left( \frac{\pi l_1}{L_1} \right) \right] + s', \quad (\text{S3})$$

where  $c$  is the central charge of the CFT and  $s'$  is a nonuniversal constant<sup>S1,S2</sup>. As shown in Fig. S8(b),  $-d^2 E_g/dh^2$  shows two relatively sharp peaks at  $\mu_B h/|K| \approx 0.045$  and  $0.095$ , and one broaden peak at  $\mu_B h/|K| \approx 0.06$ , thus supporting that there exist one or two IPs emerging also in the periodic  $2 \times 16 \times 3$  cluster. Interestingly, the obtained  $c$  value shown in Fig. S8(b) is almost zero for  $0.06 \lesssim \mu_B h/|K| \lesssim 0.09$  in the IP. This infers that the IP is gapped, which is in contrast with the  $K$ - $J$  model with antiferromagnetic  $K$  and ferromagnetic  $J$  model where the possible IP is proposed to be the gapless  $U(1)$  spin liquid with  $c = 2$ <sup>S3</sup>. In addition, we find that  $c$  has a finite value at the magnetic field around which  $-d^2 E_g/dh^2$  exhibits the relatively sharp peaks. This implies that the excitation gap is closed at the critical fields of the phase transition.

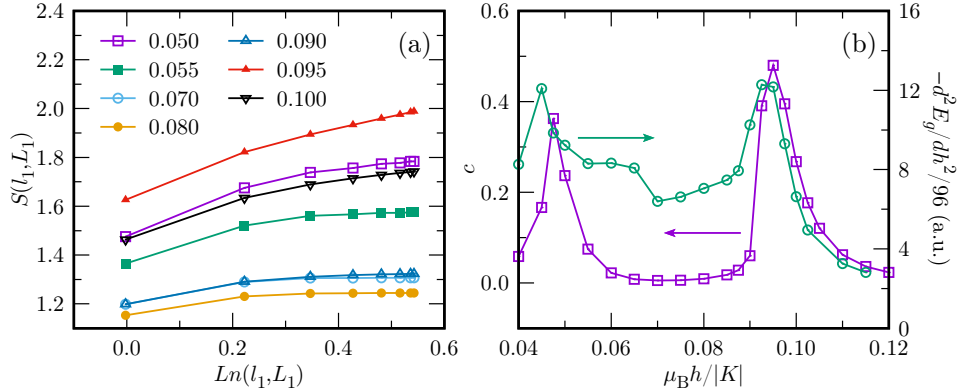


FIG. S8. (a) The Entanglement entropy (EE) as a function of the subsystem length  $l_1$  along the  $L_1$  direction for various  $c$ -axis field strengths ( $\mu_B h/|K| = 0.05, 0.055, 0.07, 0.08, 0.09, 0.095, \text{ and } 0.1$ ).  $\text{Ln}(l_1, L_1)$  in the horizontal axis is defined as  $\text{Ln}(l_1, L_1) = \frac{1}{3} \ln \left[ \frac{L_1}{\pi} \sin \left( \frac{\pi l_1}{L_1} \right) \right]$ . For  $l_1 > 2$ , the EEs are fitted reasonably well by the linear function of  $\text{Ln}(l_1, L_1)$ . (b) Second derivative of the ground state energy per site ( $d^2 E_g/dh^2/N$ ) with respect to the  $c$ -axis field  $h$  and the central charge  $c$  estimated by fitting the EEs with Eq. (S3). All results are obtained for the  $K$ - $J_3$  model with  $K < 0$  and  $J_3/|K| = 0.1$  on a periodic  $2 \times L_1 \times L_2$  cluster with  $L_1 = 16$  and  $L_2 = 3$  (thus the system size being  $N = 96$ ) calculated using the DMRG method.

[S1] S. Nishimoto, *Phys. Rev. B* **84**, 195108 (2011).

[S2] H.-C. Jiang, M. S. Block, R. V. Mishmash, J. R. Garrison, D. N. Sheng, O. I. Motrunich, and M. P. A. Fisher, *Nature* **493**, 39 (2013).

[S3] Y.-F. Jiang, T. P. Devereaux, and H.-C. Jiang, *Phys. Rev. B* **100**, 165123 (2019).